Calculation of exchange constants of III–V dilute magnetic semiconductors using a quasiparticle method

Calculation of exchange constants of III–V dilute magnetic semiconductors using a quasiparticle method

J H Cai[1] and G Q Liu[1,2]

[1] Department of Physics, Shanghai Jiaotong University, Shanghai 200030,
People's Republic of China
[2] CCAST (World Laboratory), PO Box 8730, Beijing 100080, People's Republic of China

E-mail: jhcai@sjtu.edu.cn

Abstract
A quasiparticle method based on a multisite s(p)–d mixing model is used to calculate the exchange constants of dilute magnetic semiconductors (DMS). The effective interaction, which is mediated by s(p) electrons, between d electrons, was taken into account in an effective field approximation or a coherent potential approximation (CPA). The equation-of-motion technique was applied to Green functions to calculate the quasiparticle state density. The exchange constants were calculated in a double-valence-band model, and the microscopic parameter dependences of the exchange constants are investigated for fixed valence band parameters in the model. A ferromagnetic d–d coupling is obtained when the d energy level E_d is in the vicinity of the valence band top, and an antiferromagnetic d–d coupling is obtained when E_d is in the vicinity of the valence band bottom. The maximum of the d–d exchange constant $J_{\text{dd}}(E_d)$ increases with the mixing strength. J_{dd} increases with decreasing Fermi energy E_{F}, and the effect is more significant when E_d approaches the valence band top. J_{dd} also increases with small magnetic impurity concentration x, then reaches a maximum, and finally decreases sharply when x increases further. The quasiparticle state density shows that the ferromagnetism originates from the unsymmetrical broadening of the shallow d energy level in ferromagnetic alignment and related lowering of the centre of gravity of the d state density. Relevant experimental results are discussed on the basis of our calculation.

1. Introduction

A great deal of attention has been focused on III–V dilute magnetic semiconductors (DMS) [1–4] due to their application potential in the fabrication of a different class of tunable ferromagnetic devices, which are controlled by the carrier population in a semiconductor [5–7].

There have been many efforts to achieve room temperature ferromagnetism in DMS [8–13] because of their practical importance in spintronic devices. An important way to adjust the magnetic properties of DMS is to change the combination of host material and magnetic impurity atom [14–22]. The host materials for DMS are usually (Al, In, Ga)As, GaN, TiO_2, Zn(O,Te), Sb_2Te_3, etc. The impurity atoms are V, Cr, Mn, Fe, Co, Ni, etc. At present the highest Curie temperature T_C is about 110 K in p-type $Ga_{1-x}Mn_xAs$ [23], 333 K in $In_{1-x}Mn_xAs$ [12], and 940 K in n-type $Ga_{1-x}Mn_xN$ [9]. Ferromagnetism has been obtained not only in III–V DMS, but also in other materials, such as $Sb_{2-x}V_xTe_3$ [19], $Zn_{1-x}Cr_xTe$ [21], $Ti_{1-x}Co_xO_2$ [13], and, moreover, the T_C of $Ti_{1-x}Co_xO_2$ exceeds 400 K.

Many theoretical studies have also been carried out [24–33]. An important subject in these studies is the origin of the ferromagnetism in III–V DMS. The researchers in this field have tried to use many models and/or mechanisms, such as RKKY, magnetic polaron, double-exchange, and Zener model ones, to interpret the ferromagnetism in some respects [25, 26]. It has been shown that there were difficulties in using the former two models, the RKKY and magnetic polaron ones, to explain the ferromagnetism in III–V DMS [25]. The double-exchange model was originally proposed to explain the ferromagnetism in mixed-valence manganites of perovskite structure [34, 35], such as $(La_xCa_{1-x})(Mn_x^{III}Mn_{1-x}^{IV})O_3$, but it may be not suitable for DMS since the Mn atoms are impurities in DMS and the Mn atoms in the two systems are not on an equal footing. The primary support for the double-exchange model for DMS comes from *ab initio* calculations [25, 31–33]. The Zener model was originally advanced for the ferromagnetism in transition metals [36]. Dietl *et al* have calculated T_C using the Zener model for various DMS, and obtained two important results [26]: (i) the T_C of $Ga_{1-x}Mn_xN$ is above room temperature; and (ii) T_C increases with the p-type carrier density. The first result has been realized in experiments, and the second result also has been verified by a large number of experiments. The Zener model is the most successful one among these models.

Although a considerable amount of experimental data have already been accumulated and many theoretical studies have been made, there are still some experimental results which are difficult to understand within the framework of existing models. For Mn-doped GaN, three controversial results were reported. Zajac *et al* observed antiferromagnetic ordering with $T_N = 2.4$ K in $Ga_{1-x}Mn_xN$ [14]. Kuwabara *et al* obtained a paramagnetic $Ga_{1-x}Mn_xN$ epilayer with a paramagnetic Curie temperature $\theta_p = 20$ K [15] and Szyszko *et al* also obtained paramagnetism in single-crystal $Ga_{1-x}Mn_xN$ [16]. Theodoropoulou *et al* [37], Reed *et al* [8], and Sonoda *et al* [9] reported ferromagnetism in $Ga_{1-x}Mn_xN$ with values of T_C of 250, 228–370, 940 K, respectively. The physics behind these controversial results is not understood.

According to the Dietl *et al* calculation based on the Zener model, T_C should increase with the carrier density [26]. There are also controversial results on this point in experimental findings. Fukuma *et al* [22] observed carrier-enhanced ferromagnetic order in $Ge_{1-x}Mn_xTe$ and Matsukura *et al* [38] showed carrier-enhanced ferromagnetism using electric field control in a field-effect transistor structure. However, Pearton *et al* found that the use of superlattices to enhance the hole concentration did not produce any change in the ferromagnetic ordering temperature in p-AlGaN/GaN superlattices after implantation with high doses $(3–5 \times 10^{16}$ cm$^{-2})$ of Mn, Fe, or Ni [20] and Slupinski *et al* found that the hole concentration sufficient for producing $T_C = 50$ K for $In_{1-x}Mn_xAs$ [39] is several times lower than the value from the existing theory [26]. These facts indicate that the free carrier may not be responsible for the high ferromagnetism transition temperature of DMS. Litvinov and Dugaev [30] made calculations for the indirect exchange interaction caused by virtual electron excitations from the magnetic impurity acceptor level to the valence band for the interpretation of ferromagnetism in III–V DMS. Dietl *et al* [27] also showed that a high T_C above room temperature is obtained

for a low hole density in the Zhang–Rice limit. The two theoretical calculations are helpful for understanding the role of free carriers; however, the controversial results on this point from experiments still require further theoretical clarification. These experimental results also show that the properties of III–V DMS are sensitive to their fabrication conditions or, alternatively, the microscopic electronic structure parameters. A strong correlation between the location of Mn sites and the Curie temperature has been found for ferromagnetic $Ga_{1-x}Mn_xAs$ [40]. The experimental result indicates that it is necessary to study the dependence of the d–d exchange interaction on the microscopic electronic structure parameters theoretically.

There are also controversial points in some existing models. In the double-exchange model, the d hole is an important factor for obtaining ferromagnetism. In complete contrast to the double-exchange model, the Zener model [26, 36] treats all d electrons of Mn atoms as having spin S, and the possibility for d electrons to possess partially extended characteristics is removed. In some cases, one may want to calculate the p–d exchange constant, the spin polarization of the valence electron, and their temperature behaviours [41], but it is inconvenient to start from two models.

In this paper a quasiparticle method for calculating the exchange constants of DMS is developed on the basis of a more general microscopic model (the s(p)–d mixing model) [42] and our previous work [43], and the exchange interaction in III–V DMS is investigated within a double-valence-band model. In this method, first the quasiparticle energy and occupation number are calculated from the s(p)–d mixing model Hamiltonian; then the relationship between the exchange constants and these microscopic quantities is constructed, and hence exchange constants are obtained. It will be revealed that the d–d exchange constant depends on the position of the d level in the valence band of the host, the strength of the s(p)–d mixing, the Fermi energy level E_F, and the mean distance between magnetic atoms. Although the free carrier concentration and the Fermi energy level affect the exchange interplay, they are not decisive factors as regards achieving ferromagnetism; hence ferromagnetism can be obtained in a p-type DMS as well as in a n-type DMS, and even in an insulator-like DMS.

The paper is organized as follows. Section 2 gives the formulae used to calculate the exchange constants of DMS. In section 3, some general considerations on these formulae are presented, and the concepts of resonant momentum and phase factor are also introduced. The microscopic parameter dependence of the exchange constants and related discussions are presented in section 4. The results obtained are summarized in section 5.

2. Method of calculation

In this section the method used to calculate the exchange constants from the multisite s(p)–d mixing model Hamiltonian [44] is presented. The calculation procedure can be divided into two steps. The first step is the calculation of the quasiparticle energy and the occupation number from the multisite s(p)–d mixing model Hamiltonian for a magnetic configuration, and the second step is the calculation of the exchange constants using the quasiparticle energy and occupation number. We will describe the method in two steps.

2.1. Calculation of the quasiparticle energy and occupation number

We start from the multisite s(p)–d mixing model Hamiltonian [44]

$$\hat{H} = \sum_{di\sigma} E_d \hat{n}_{di\sigma} + \frac{1}{2} \sum_{di\sigma} U_d \hat{n}_{di\sigma} \hat{n}_{di\overline{\sigma}} + \sum_{nk\sigma} E^e_{nk} \hat{c}^\dagger_{nk\sigma} \hat{c}_{nk\sigma}$$
$$+ \frac{1}{\sqrt{N}} \sum_{dink\sigma} (T_{dn\sigma} e^{i\vec{k}\cdot\vec{r}_i} \hat{a}^\dagger_{di\sigma} \hat{c}_{nk\sigma} + T^*_{dn\sigma} e^{-i\vec{k}\cdot\vec{r}_i} \hat{c}^\dagger_{nk\sigma} \hat{a}_{di\sigma}), \tag{1}$$

where N denotes the total number of lattice points, i denotes the ith lattice point occupied by a 3d impurity atom, and the sum over i extends over only the sites occupied by 3d impurity atoms. The subscript d denotes local d energy level, n the energy band, k the momentum, and σ the spin. $\hat{a}_{di\sigma}^{\dagger}$ ($\hat{a}_{di\sigma}$) is the creation (annihilation) operator for a local d electron, and $\hat{c}_{nk\sigma}^{\dagger}$ ($\hat{c}_{nk\sigma}$) is the creation (annihilation) operator for an extended s(p) electron. In equation (1) the first and second terms describe d electrons with a Hubbard repulsion energy U_d. The third term describes s(p) band electrons in the host. The last term describes the mixing of d electrons with s(p) electrons via a parameter $T_{dn\sigma}$. In a general case, $T_{dn\sigma}$ should depend on momentum k; however, its k dependence can be neglected as shown by Larson *et al* [45]. We will also give a brief discussion of the neglect of the k dependence in section 3.

In the paper the equation-of-motion method is adopted to calculate retarded single-particle thermodynamical Green functions; then the quasiparticle energy and occupation number are obtained from the Green functions. The formulae are presented here in an intuitive manner, and the details of the derivation procedure relevant to Green functions are given as a supplement in appendix A.

Applying the Hartree–Fock approximation to equation (1), we obtain the Green function $\langle\langle\hat{a}_{di\sigma}|\hat{a}_{d'i'\sigma'}^{\dagger}\rangle\rangle$ from the following equation:

$$(\omega - e_{di\sigma})\langle\langle\hat{a}_{di\sigma}|\hat{a}_{d'i'\sigma'}^{\dagger}\rangle\rangle = \delta_{di\sigma,d'i'\sigma'} + \sum_{d_1 i_1 \neq di} f_{di,d_1 i_1}(\sigma)\langle\langle\hat{a}_{d_1 i_1 \sigma}|\hat{a}_{d'i'\sigma'}^{\dagger}\rangle\rangle, \quad (2)$$

where

$$e_{di\sigma} = E_{\rm d} + U_d\langle\hat{n}_{di\overline{\sigma}}\rangle + \frac{1}{N}\sum_{nk}\frac{|T_{dn\sigma}|^2}{\omega - E_{nk}^e}, \quad (3)$$

$$f_{di,d_1 i_1}(\sigma) = \frac{1}{N}\sum_{nk}\frac{T_{dn\sigma}T_{d_1 n\sigma}^* {\rm e}^{{\rm i}\vec{k}\cdot(\vec{r}_i - \vec{r}_{i_1})}}{\omega - E_{nk}^e}. \quad (4)$$

In equations (3) and (4), ω should contain an infinitely small imaginary part $i0^+$ for a retarded Green function, and this convention will be used throughout this paper.

The effective interaction between two d electrons at lattice points i and i_1 is taken into account via $f_{di,d_1 i_1}$ in equation (2). A possible method for resolving equation (2) is the perturbative approach, directly using $(\omega - e_{di\sigma})^{-1}$ as the propagator. However, the perturbative solution to equation (2) is not adequate for us to calculate exchange constants in a situation with a shallow d energy level. The perturbative approach breaks down when $\rho_{nk}^e T_{dn\sigma} T_{d_1 n\sigma}^*$ (ρ_{nk}^e is the density of valence states $|nk\rangle$) is not a small quantity [46]. According to Larson's estimation, $T_{dn\sigma}$ is about 0.8 eV for an electron in the vicinity of the valence edge $E_{\rm v}$ [45]. In the case of a narrow valence band, $\rho_{nk}^e T_{dn\sigma} T_{d_1 n\sigma}^*$ may not be a small quantity. Even if the perturbative approach is suitable for calculating the quasiparticle energy, it may be not suitable for calculating the difference between various magnetic configurations since $\rho_{nk}^e(\omega)$ shows a sharp change with ω when it approaches $E_{\rm v}$.

The above viewpoint as regards the perturbative solution to equation (2) can be elucidated through a simplified model problem. Equation (2) can be regarded as a solution to an effective Hamiltonian:

$$\hat{H}_{\rm eff} = \sum_{di\sigma} e_{di\sigma}\hat{a}_{di\sigma}^{\dagger}a_{di\sigma} + \sum_{\langle di,d_1 i_1\rangle\sigma} f_{di,d_1 i_1}(\sigma)a_{di\sigma}^{\dagger}a_{d_1 i_1 \sigma} \quad (5)$$

if the dynamical dependence of $f_{di,d_1 i_1}$ is neglected and $f_{di,d_1 i_1}$ becomes a real number. If a superlattice limit and only the nearest-neighbour hopping terms are considered, the effective Hamiltonian can be regarded as a conventional tight binding Hamiltonian (TBH) for a fixed ω. From knowledge about the conventional TBH, we know that any finite order perturbation using

$(\omega - e_{di\sigma})^{-1}$ as the propagator for this effective Hamiltonian is inadequate for characterizing its essential extended state nature, so we should consider another approximation method.

Following the idea of a coherent potential approximation (CPA) for a disordered alloy [47], we replace the free propagator $(\omega - e_{di\sigma})^{-1}$ with an effective propagator $[\omega - \Sigma(di\sigma)]^{-1}$ in the second-order perturbative solution to equation (2), and the corresponding self-energy $\Sigma(di\sigma)$ of $\langle\langle \hat{a}_{di\sigma} | \hat{a}_{d'i'\sigma'}^{\dagger}\rangle\rangle$ is written as

$$\Sigma(di\sigma) = e_{di\sigma} + \sum_{d_1 i_1 \neq di} \left\langle \frac{f_{di,d_1 i_1}(\sigma) f_{d_1 i_1, di}(\sigma)}{\omega - \Sigma(d_1 i_1 \sigma)} \right\rangle. \tag{6}$$

$\langle \cdots \rangle$ in equation (6) denotes the average over a random distribution of magnetic atoms. Besides this meaning, here the CPA has another important interpretation: in this coherent field, the contributions of the scattering of order higher than the fourth cancel each other out, and equation (6) provides a self-consistent condition for determining the self-energy. The latter places the CPA beyond the conventional perturbative approximation, and this point will be discussed further. The details about the averaging over a random distribution are given as a supplement in appendix B.

If the free propagator $(\omega - e_{di\sigma})^{-1}$ in the second-order perturbative solution to the Green function $\langle\langle c_{nk\sigma} | c_{nk\sigma}^{\dagger}\rangle\rangle$ is replaced with the effective propagator $[\omega - \Sigma(di\sigma)]^{-1}$, a CPA solution to the Green function of the s(p) band electron is obtained as

$$\langle\langle c_{nk\sigma} | c_{nk\sigma}^{\dagger}\rangle\rangle = \left(\omega - E_{nk}^{e} - \frac{1}{N}\sum_{di} \frac{|T_{dn\sigma}|^2}{\omega - \Sigma(di\sigma)} \right)^{-1}. \tag{7}$$

The valence electrons are scattered by d electrons in a coherent field, so their lifetime becomes finite and they may be spin polarized. The self-energy correction term $\frac{1}{N}\sum_{di} \frac{|T_{dn\sigma}|^2}{\omega - \Sigma(di\sigma)}$ in equation (7) takes the above two points into account. On the basis of the same consideration, the self-energy correction term is also inserted in equation (4), so equation (4) is rewritten as

$$f_{di,d_1 i_1}(\sigma) = \frac{1}{N}\sum_{nk} \frac{T_{dn\sigma} T_{d_1 n\sigma}^{*} e^{i\vec{k}\cdot(\vec{r}_i - \vec{r}_{i_1})}}{\omega - E_{nk}^{e} - \frac{1}{N}\sum_{di} \frac{|T_{dn\sigma}|^2}{\omega - \Sigma(di\sigma)}}. \tag{8}$$

In equation (6) the energy of interaction between d electrons is explicitly taken into account, so the d quasiparticle energy depends on the relative orientation of local spins. Once the type of magnetic coupling is known, the Green functions of d and s(p) electrons can be obtained from the above formulae, and the density of quasiparticles ($\rho_{d\sigma}(\omega)$, $\rho_{nk\sigma}(\omega)$) is obtained from the Green function according to the spectrum theorem; then the quasiparticle energy and occupation number are obtained via the following formulae:

$$\begin{aligned} \langle E_{d\sigma} \rangle_M &= \int \omega \rho_{d\sigma}^{M}(\omega) f(\omega) \, d\omega, \\ \langle n_{d\sigma} \rangle_M &= \int \rho_{d\sigma}^{M}(\omega) f(\omega) \, d\omega, \\ \langle E_{nk\sigma} \rangle_M &= \int \omega \rho_{nk\sigma}^{M}(\omega) f(\omega) \, d\omega, \\ \langle n_{nk\sigma} \rangle_M &= \int \rho_{nk\sigma}^{M}(\omega) f(\omega) \, d\omega, \end{aligned} \tag{9}$$

where $f(\omega)$ is the Fermi–Dirac distribution function, and the label M denotes a particular magnetic configuration.

2.2. Calculation of exchange constants

After the procedure of statistical averaging has been carried out, an ordered sublattice can be used to calculate some macroscopic quantities (e.g. T_C), since the disorder effect has been taken into account in the calculable quantities in the s(p)–d mixing model. It is assumed that the sublattice has an enlarged lattice constant $a/x^{1/3}$ (a is the lattice constant of the host; x is the concentration of impurity atoms) and the same symmetry elements as the host lattice. If local moments exist in the DMS, the coupling between local magnetic moments can be described by the Heisenberg Hamiltonian

$$\hat{H}_{\mathrm{h}} = -J_{\mathrm{dd}} \sum_{\langle ij \rangle} \hat{\vec{S}}_i \cdot \hat{\vec{S}}_j. \tag{10}$$

Here the sum over i and j extends over the sites in the order sublattice, and the exchange constant J_{dd} should be understood in the sense of statistical averaging. If the relationship between the exchange constants and the calculable quantities in the s(p)–d mixing model is constructed, we can calculate the exchange constants via the calculation of the corresponding quantities in the s(p)–d mixing model. As all the methods are based on a microscopic Hamiltonian, the relationship between equations (1) and (10) is also constructed from the energy aspect. In the kinetic approach [45], a fourth-order perturbative matrix element connecting two different spin states for the mixing term in equation (1) is treated as the equivalent quantity connecting the two Hamiltonians. In other approaches, the difference in total energy [48] or free energy [26] between two magnetic configurations is treated as an equivalent difference between the two Hamiltonians. In our approach, quasiparticle energy is employed to construct the relationship between the two Hamiltonians.

For convenience, an operator

$$\hat{H}_{\mathrm{h}}(i) = -2J_{\mathrm{dd}} \sum_{\delta \neq 0} \hat{\vec{S}}_i \cdot \hat{\vec{S}}_{i+\delta} \tag{11}$$

is introduced; then the Heisenberg Hamiltonian can be written in a concise form: $\hat{H}_{\mathrm{h}} = \sum_i \hat{H}_{\mathrm{h}}(i)$. For a particular magnetic configuration M_i, where the angle between the nearest-neighbour moments is θ_i, equation (11) is written as

$$\langle \hat{H}_{\mathrm{h}}(0) \rangle_{M_i} = -\tfrac{1}{2} J_{\mathrm{dd}} z \left[\sum_d (\langle n_{d\uparrow} \rangle_{M_i} - \langle n_{d\downarrow} \rangle_{M_i}) \right]^2 \cos \theta_i \tag{12}$$

in the mean field approximation. Here z is the mean number of nearest-neighbour magnetic atoms in the sublattice. Without loss of generality, we use $z = 6$, as for the host lattice, in the following actual calculation. The assumption as regards the value of z does not affect the evaluation of the Curie point T_C since T_C is determined by $J_{\mathrm{dd}} z$, which is equivalent to J_0 in the Liechtenstein et al paper [48], not z only. Because $\langle E_{d\sigma} \rangle_{M_i}$ contains the single-particle energy besides the interaction energy, and $\langle \hat{H}_{\mathrm{h}}(0) \rangle_{M_i}$ contains only the interaction energy, the relationship between $\langle E_{d\sigma} \rangle_{M_i}$ and $\langle \hat{H}_{\mathrm{h}}(0) \rangle_{M_i}$ can be constructed via the following equation:

$$\sum_{d\sigma} \langle E_{d\sigma} \rangle_{M_i} = \langle \hat{H}_{\mathrm{h}}(0) \rangle_{M_i} + c \sum_{d\sigma} \langle n_{d\sigma} \rangle_{M_i} \qquad (i = 1, 2), \tag{13}$$

where c is a constant independent of the magnetic configuration. Given any two configurations, the constant c can be cancelled, so the exchange constant J_{dd} is obtained. In the following numerical calculation, a ferromagnetic (F) configuration ($\theta_1 = 0$) and an antiferromagnetic (AF) configuration ($\theta_2 = \pi$) are used to calculate J_{dd} for a negative J_{dd}, and a F configuration ($\theta_1 = 0$) and a canted ferromagnetic ($\theta_2 = 0.3\pi$) one are used to calculate J_{dd} for a positive J_{dd}.

Because equation (10) is applicable only for small spin deviations from the ferromagnetic ground state [48] and numerical stability requires spin deviations that are not too small, a small and finite $\theta_2 = 0.3\pi$ is adopted for ferromagnetic coupling in actual calculations.

The method used to calculate $J_{\rm dd}$ using equation (13) is consistent with an existing method [48, 49]. When the variation of $\sum_{d\sigma} \langle n_{d\sigma} \rangle$ between two magnetic configurations is small enough, equation (13) is equivalent to $\sum_{d\sigma} \langle E_{d\sigma} \rangle_{M_1} - \sum_{d\sigma} \langle E_{d\sigma} \rangle_{M_2} = \langle \hat{H}_{\rm h}(0) \rangle_{M_1} - \langle \hat{H}_{\rm h}(0) \rangle_{M_2}$. Alternatively, we can use the quasiparticle energy variation to determine $J_{\rm dd}$. This should be an acceptable approximation [49], since it has been proved that the total energy variation coincides with the sum of one-particle energy changes for the occupied states at the fixed ground state potential [48].

Because the calculation in this paper is done at a fixed Fermi energy, the occupation number may change with the magnetic configuration. In order to eliminate this effect, we introduce a constant c in equation (13). According to density functional theory, the non-interactive part of the quasiparticle energy can be expressed as a function of $\sum_{d\sigma} \langle \hat{n}_{d\sigma} \rangle$. Constructing a power series expansion to the function and omitting terms higher than the second-order ones, we can write the non-interactive part of the quasiparticle energy in the form $c \sum_{d\sigma} \langle \hat{n}_{d\sigma} \rangle$. Hence the constant c in equation (13) comes from a linear approximation to the non-interactive part of the quasiparticle energy, and the introduction of c can eliminate the effect due to occupation number change with magnetic configuration to a certain extent.

An analogous procedure is used to obtain $J_{\rm s(p)-d}$. The s(p)–d exchange Hamiltonian

$$\hat{H}_{\rm s(p)-d} = -\tfrac{1}{2} \sum_{nkk'i\sigma\sigma'} J^n_{\rm s(p),d}(k, k') \hat{\vec{S}}_i \cdot \hat{c}^\dagger_{nk\sigma} \vec{\sigma}_{\sigma\sigma'} \hat{c}_{nk'\sigma'} {\rm e}^{{\rm i}(\vec{k}-\vec{k}')\cdot\vec{r}_i} \tag{14}$$

is usually used to describe the coupling between local magnetic moments and itinerant electrons. An operator

$$\hat{H}_{\rm s(p)-d}(nk\sigma) = -\tfrac{1}{2} \sum_i J^n_{\rm s(p),d}(k, k) \hat{\vec{S}}_i \cdot \hat{c}^\dagger_{nk\sigma} \vec{\sigma}_{\sigma\sigma} c_{nk\sigma} \tag{15}$$

is also introduced to simplify the expression, but only a ferromagnetic configuration is considered for the calculation of $J^n_{\rm s(p),d}$ [45]. The energy difference between $\langle \hat{H}_{\rm s(p)-d}(nk\downarrow) \rangle_{\rm F}$ and $\langle \hat{H}_{\rm s(p)-d}(nk\uparrow) \rangle_{\rm F}$ is written as

$$\begin{aligned}
\langle \hat{H}_{\rm s(p)-d}(nk\downarrow) \rangle_{\rm F} &- \langle \hat{H}_{\rm s(p)-d}(nk\uparrow) \rangle_{\rm F} \\
&= \tfrac{1}{2} xNS J^n_{\rm s(p),d}(k, k) \sum_d \langle \hat{n}_{d\uparrow} - \hat{n}_{d\downarrow} \rangle_{\rm F} \langle \hat{n}_{nk\uparrow} + \hat{n}_{nk\downarrow} \rangle_{\rm F}
\end{aligned} \tag{16}$$

in the mean field approximation. Here x is the concentration of magnetic atoms, xN is the population of magnetic atoms, and the label F denotes a ferromagnetic configuration. The relationship between $\langle E_{nk\sigma} \rangle_{\rm F}$ and $\langle \hat{H}_{\rm s(p)-d}(nk\sigma) \rangle_{\rm F}$ has a simple form:

$$\langle E_{nk\downarrow} \rangle_{\rm F} - \langle E_{nk\uparrow} \rangle_{\rm F} = \langle \hat{H}_{\rm s(p)-d}(nk\downarrow) \rangle_{\rm F} - \langle \hat{H}_{\rm s(p)-d}(nk\uparrow) \rangle_{\rm F}, \tag{17}$$

and finally the s(p)–d exchange constant $J^n_{\rm s(p),d}$ is also obtained.

3. General considerations on formulae

3.1. f_{di,d_1i_1} and the phase factor effect

In our calculation method, the effect of correlation between magnetic atoms is included via f_{di,d_1i_1} in equation (4) or (8). According to equation (2), f_{di,d_1i_1} can be interpreted as a dynamical effective overlap integral, and $|f_{di,d_1i_1}|^2$ is proportional to the probability of an
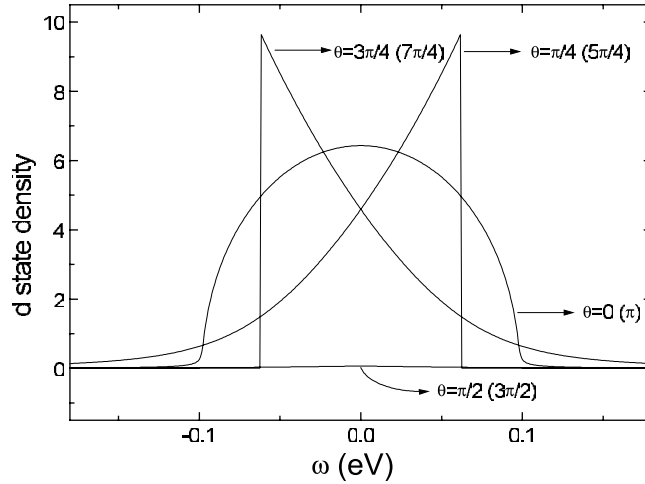
Figure 1. An illustration of the effect of the phase factor on the local density. A simple cubic superlattice is assumed for sites occupied by magnetic atoms, and $|f_{di,d_1i_1}| = 0.02$ eV for the nearest-neighbour site pairs and $|f_{di,d_1i_1}| = 0$ for other site pairs. A lower centre of gravity of the local density is obtained in the situations with $\theta = 0$ (π) and $3\pi/4$ ($7\pi/4$).

electron going from state $|d_1i_1\sigma\rangle$ to state $|di\sigma\rangle$; hence f_{di,d_1i_1} can also be interpreted as a transition probability amplitude.

Since f_{di,d_1i_1} is a complex number, its phase factor plays an important role in the determination of the exchange type, ferromagnetic or antiferromagnetic. We will see this from a simplified case. We suppose that the sites occupied by magnetic atoms form a superlattice with a simple cubic structure and that f_{di,d_1i_1} is a nonzero complex constant (its dependences on ω and Σ are neglected here) for the nearest-neighbour sites i and i_1, and zero for other site pairs. Denoting the nonzero complex constant f_{di,d_1i_1} as $|f|e^{i\theta}$ and supposing that $e_{di\sigma} = 0$, we study the characteristic of the local density determined by equation (6) for various phase factors. Figure 1 shows the local density for $|f| \neq 0$ and the phase factor $\theta = 0$ (π), $\pi/4$ ($5\pi/4$), $\pi/2$ ($3\pi/2$), and $3\pi/4$ ($7\pi/4$). Because the local density for $|f| = 0$ has no structure except an isolated peak at $\omega = 0$, it is not shown in figure 1. The centre of gravity of the local density for $\theta = 0$ (π) becomes lower in comparison with that for $|f| = 0$ if the state is partly filled. For $\theta = 3\pi/4$ ($7\pi/4$), the centre of gravity of the local density is lower, without any extra conditions. The two cases facilitate ferromagnetic exchange in the simplified examples.

A straightforward way to verify the effect of the phase factor on the exchange constant is to study the relationship of the phase factor with the position of the positive maximum point of the $J_{dd}(E_d)$ curve in a single-valence-band model with a dispersion relation $E(\vec{k}) = -(W/2) + (W/6)\sum_{i=0}^{3}\cos(k_ia)$ (W is the bandwidth; a is the lattice constant). For a given E_d, the primary contributions to f_{di,d_1i_1} come from the valence electrons with energy $E(\vec{k}) = E_d$. The corresponding momentum of the valence electron may be called the resonant momentum, $\vec{k}_{res}$. In the approximation of nearly free electrons, the magnitude of the resonant momentum can be estimated from $E_d = -(W/12)(k_{res}a)^2$. If $\bar{r}$ denotes the mean distance between the nearest-neighbour magnetic atoms, $|k_{res}|\bar{r}$ can be regarded as a certain measure of the phase factor θ. The E_d, $|k_{res}|$, and $|k_{res}|\bar{r}$ corresponding to the positive maximum of $J_{dd}(E_d)$ for various valence bandwidths W are listed in table 1. Although E_d (the position of the maximum point) depends on W, $k_{res}\bar{r}$ is almost a constant, 0.88π, which is between $3\pi/4$ and π. This is consistent with the above discussion of phase factors. It should

Table 1. The corresponding values of E_d, $|k_{res}|$, and $|k_{res}|\bar{r}$ when $J_{dd}(E_d)$ reaches a positive maximum point for various values of W. W is the width of a simple cubic valence band, and its top is at the zero point. The parameters in the calculation of J_{dd} are $T = 0.1$ K, $E_F = 0.0$ eV, $U_d = 7.0$ eV; the s(p)–d mixing parameter $T_{dn\sigma} = 0.2$ eV. $|k_{res}|\bar{r}$ approaches a constant, 0.88π.

W (eV)	E_d (eV)	$|k_{res}|$ $(1/a)$	$|k_{res}|\bar{r}$
2.0	−0.22	1.14	0.91π
2.5	−0.24	1.07	0.85π
3.0	−0.30	1.09	0.87π
3.5	−0.36	1.11	0.88π
4.0	−0.36	1.10	0.88π

be mentioned here that this phase factor effect is a quantum interference effect in essence, and the effect can be used to tailor the magnetic properties of DMS.

3.2. $T_{dn\sigma}$ and the k-dependence

We have mentioned that in a general case $T_{dn\sigma}$ should depend on the momentum k and it may be denoted by $T_{dn\sigma}(\vec{k})$. The concept of resonant momentum facilitates the understanding of the neglect of the k dependence of the mixing parameter $T_{dn\sigma}(\vec{k})$. For a fixed E_d, the dominant contributions to $f_{di,d_1 i_1}$ come from the resonant valence electrons and therefore a value averaged over the $\vec{k}$ points at the surface $E(\vec{k}) = E_d$ can be adopted if the anisotropies of the exchange constants are not considered. In this paper, $N J^n_{s(p),d}(k, k)$ is also calculated, in addition to J_{dd}. Because the k in $N J^n_{s(p),d}(k, k)$ is usually different from the resonant momentum k_{res}, a different value for $T_{dn\sigma}$ should be used in equation (7). According to Larson's results, $T_{dn\sigma}(\vec{k})$ at $k = 0$ is about four times the corresponding mean value in II–VI DMS [45]. So four times $T_{dn\sigma}$ replaces $T_{dn\sigma}$ in equation (7) when $N J^n_{s(p),d}(0, 0)$ is calculated. In Larson's paper this substitution is also used to determine $T_{dn\sigma}$ from $N J^n_{s(p),d}(0, 0)$ [45].

Briefly, a parameter $T_{dn\sigma}$ independent of k can be used to calculate exchange constants if we remember that a different value, e.g. four times $T_{dn\sigma}$, of $T_{dn\sigma}$ in equation (7) should be used in the calculation of $N J^n_{s(p),d}(0, 0)$.

4. Results and discussion based on a double-valence-band model

4.1. The double-valence-band model

In this paper a double-valence-band model, in which a simple cubic dispersion relation $E^e_{nk} = E_n + 2T_n \sum_{i=1}^{3} \cos(k_i a)$ (a is the lattice constant, E_n is the energy band centre or the on-site energy, and T_n is the overlap integral) is adopted, is used to calculate exchange constants and their various parameter dependences. In this paper, we concentrate our attention on situations where E_d is in the range from the valence band top to −4.0 eV below the valence band top and the gap is not too small. Because E_d is out of the conduction band, the main contribution to $f_{di,d_1 i_1}$ comes from valence bands (see appendix C). The upper valence bands of the semiconductors with a zinc-blende structure consist of three energy bands: one wide band and two narrow bands [50]. Due to spin–orbit coupling, the wide band shifts down by Δ with respect to the two narrow bands. Δ is valence split, and dependent on the actual material. For example, Δ is about 0.34 eV for GaAs, and 1.0 eV for CdTe. The two narrow bands can be treated as two degenerate bands if the difference between the dispersions along directions such as $\Gamma \rightarrow K$ is neglected. So we can use one band to represent the two narrow bands if the corresponding mixing parameter is enlarged to $\sqrt{2}$ times original value, and use the other band to represent the wide band.
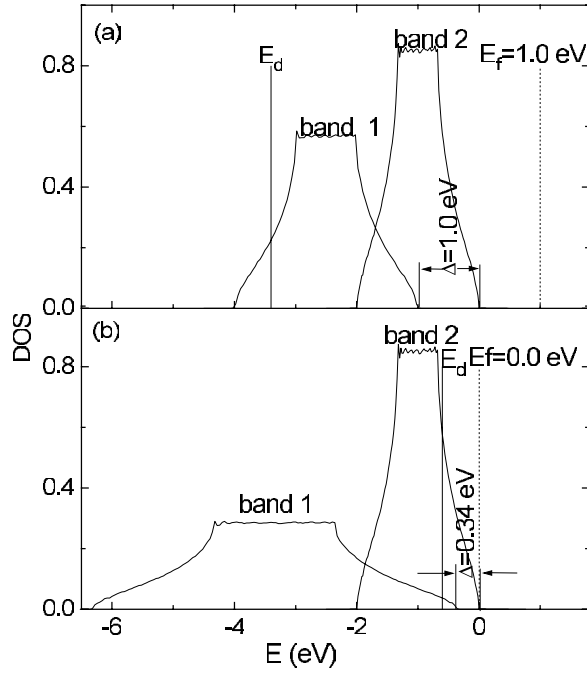
Figure 2. A schematic illustration of the valence band structure in the two-valence-band model. Two bands in panel (a) and panel (b) are intended to model the valence bands of n-CdTe ($E_F = 1.0$ eV) and p-GaAs ($E_F = 0.0$ eV), respectively. The positions of E_d are suitable for Mn-doped DMS, but E_d will sweep from -4.0 to -0.20 eV in our calculation.

In order to find appropriate values for parameters E_n and T_n, we should consider the basic characteristic of the valence band for a particular material. In this paper our main task is to study the exchange interaction in III–V DMS. In order to test the quasiparticle method and to understand why ferromagnetism can be obtained in III–V DMS, exchange constants of II–VI DMS are also calculated. So we chose CdTe and GaAs as two typical host materials for II–IV DMS and III–V DMS, respectively, to determine model parameters. A schematic illustration of the valence band is shown in figure 2. Two bands with parameters $E_1 = -2.5$ eV, $T_1 = 0.25$ eV and $E_2 = -1.0$ eV, $T_2 = 1/6$ eV are used for CdTe [50–52], and two bands with parameters $E_1 = -3.34$ eV, $T_1 = 0.5$ eV and $E_2 = -1.0$ eV, $T_2 = 1/6$ eV are used for GaAs [50, 53]. It should be mentioned that we should also consider the characteristic of the valence state density besides dispersions when we set model parameters for a particular material. For example, the width of the wide band branch in CdTe is about 3.5 eV [51] (-4.5 to -1.0 eV) or 4.0 eV [50] (-5.0 to -1.0 eV) determined from $E(k)$, but the valence state density of CdTe shows a valley at about $E = -3.5$ eV [50, 52], so a band with width 3.0 eV (-4.0 to -1.0 eV) is used in figure 2. In addition, E_F is also shown in figure 2. $E_F = 1.0$ eV in panel (a) and $E_F = 0.0$ eV in panel (b) indicate that an n-type and a p-type host semiconductor are considered here, respectively.

In the vicinity of the valence band edge or bottom, we can use the effective mass approximation to E_{nk} in equation (8), and an analytical expression (see appendix C):

$$f_{di,d_1 i_1} = \sum_n \frac{T_{dn\sigma} T_{d_1 n\sigma}^*}{T_n} \frac{e^{ik_n |\vec{r}_{i_1} - \vec{r}_i|}}{4\pi |\vec{r}_{i_1} - \vec{r}_i|}, \qquad \text{Im}(k_n) > 0, \qquad (18)$$
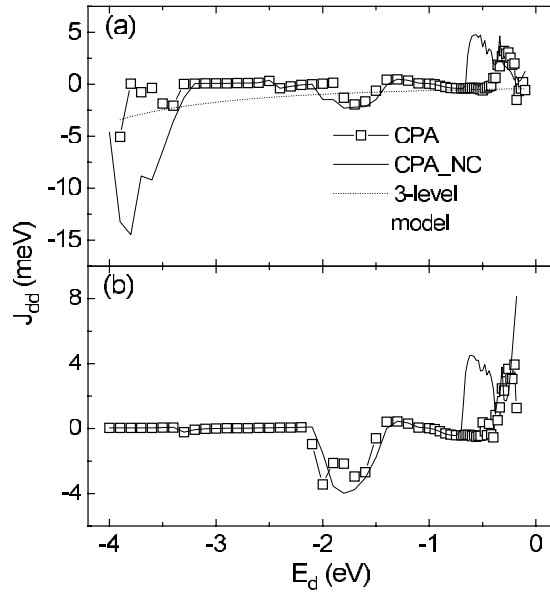
Figure 3. The exchange constant J_{dd} as a function of E_d. CPA denotes our CPA result, CPA_NC denotes our CPA result without the impurity scattering correction in $f_{di,d_1 i_1}$ (equation (4) instead of (8)). Three-level model denotes the result according to Larson's three-level model. Antiferromagnetism is obtained for E_d in the vicinity of the band bottom, and ferromagnetism is obtained for E_d in the vicinity of the band top. The parameters for the valence band used for panels (a) and (b) are the same as those used for figures 2(a) and (b), respectively. Other parameters are $T = 0.1$ K, $U_d = 7.0$ eV; the s(p)–d mixing parameter $T_{d1\sigma} = 0.2$ eV [45][3], and $T_{d2\sigma} = \sqrt{2}T_{d1\sigma}$. The 3d magnetic impurity concentration x is 6.4%.

is obtained for equation (8). Here k_n is the pole on the upper complex half-plane of k for energy band n, and has been called the resonant momentum in the above section. The multiplier $e^{ik_n|\vec{r}_{i_1} - \vec{r}_i|}$ in equation (18) guarantees that $f_{di,d_1 i_1} f_{d_1 i_1, di}$ decays more rapidly, or at least not slower, than $|\vec{r}_{i_1} - \vec{r}_i|^{-2}$; hence only the nearest-neighbour impurity points are to be considered in the sum on i_1 in equation (6). Because only those electrons at a local level near the Fermi energy E_F have a significant polarization of a valence electron, only one d level is considered in our actual calculation.

In the following context, the microscopic parameter (E_d, $T_{dn\sigma}$, E_F, mean distance between magnetic impurities) dependences of the exchange constant are investigated in the double-valence-band model where the valence band parameters are fixed, and discussions of relevant experimental results are also presented.

4.2. The E_d dependence of J_{dd} and $J_{s(p),d}$

Figure 3 shows the E_d dependence of J_{dd} in the double-valence-band model. An antiferromagnetic coupling is obtained for E_d in the vicinity of the band bottom, and a ferromagnetic coupling is obtained for E_d in the vicinity of the band top. The calculated J_{dd} for II–VI DMS is consistent with Larson's three-level model for E_d, around -3.4 eV. Compared with Larson's model, the magnitude of J_{dd} decreased more rapidly with E_d and

---

[3] Due to spin–orbit coupling, $T_{dn\uparrow} \neq T_{dn\downarrow}$ in a strict way, but we can set $T_{dn\uparrow} = T_{dn\downarrow}$ since only the up-spin branch of the d state is filled due to strong Hubbard repulsion.

shows a plateau in the range from -4.0 to -0.20 eV except for the peaks located at the band bottom or top. As anticipated in our previous discussion, ferromagnetism is obtained for shallow d energy levels; however, antiferromagnetism is obtained according to the three-level model.

The maximum of J_{dd} in figure 3(b) reaches about 4.0 meV. According to the mean field formula $k_B T_C = (2z/3)[S(S+1)]J_{dd}$ for the Curie point, the corresponding Curie temperature T_C is about 140 K. The highest T_C obtained in experiments is 110 K for $Ga_{1-x}Mn_xAs$ [23]. Our calculated J_{dd} agrees well with the experimental value in scale and is also consistent with the theoretical results based on the mean field Zener model [26, 27] and other theoretical approaches [28, 30].

If the impurity scattering correction is not taken into account in f_{di,d_1i_1} (equation (4) instead of (8)), the $J_{dd}(E_d)$ curve still exhibits a basic characteristic: negative J_{dd} for E_d in the vicinity of the band bottom and positive J_{dd} for E_d in the vicinity of the band top, but shows a change in the magnitude of J_{dd} and a shift of the peak position. Comparison with the theoretical result from the three-level model at $E_d = -3.4$ eV indicates that an impurity scattering correction in f_{di,d_1i_1} may be necessary for a quantitative calculation of J_{dd}.

In experiments, E_d depends on the combination of host material and magnetic atom. A good example as regards this point is provided by Mn DMS. The d level is deep in II–VI DMS; e.g., $E_d = -3.4$ eV in $(Cd, Zn)_{0.9}Mn_{0.1}(Te, Se, S)$ [45]. However, direct measurements of the electronic states in $Ga_{1-x}Mn_xAs$ from angle resolved photoemission spectroscopy show Mn-induced states both 3–4 eV below the top of the valence band and also very near the Fermi energy [54, 55]. In the s(p)–d mixing model, shallow E_d can produce such Mn-induced states near the Fermi energy E_F. The E_d dependence of J_{dd} maybe used to explain the facts that antiferromagnetism dominates in II–VI DMS [45] and ferromagnetism emerges in III–V DMS [1–4].

E_d also depends on the experimental procedure. According to crystal field theory, E_d should depend on the site which is occupied by the magnetic atom. It has been shown that the location of Mn sites in $Ga_{1-x}Mn_xAs$ is affected by the annealing procedure [40]; therefore E_d is also changed in the procedure. We will return to this topic in the next subsection.

Figure 4 shows the E_d dependence of $NJ^2_{s(p),d}(0, 0)$. As discussed in section 3.2, two sets of $T_{dn\sigma}$ are adopted in the calculation of $J^2_{s(p),d}(0, 0)$. $T_{dn\sigma}$ for a band-edge state is about 0.8 eV for II–IV DMS [45], so $T_{dn\sigma} = 0.8$ eV is used in equation (7). The calculated $NJ^2_{s(p),d}(0, 0)$ for II–IV DMS (panel (a)) agrees well with the experimental result and the theoretical result from Schrieffer–Wolff transformation, around $E_d = -3.4$ eV [46]. The experimental value of $NJ^2_{s(p),d}(0, 0)$ for III–V DMS is about 1.0–3.3 eV [56]. The calculated $NJ^2_{s(p),d}(0, 0)$ (panel (b)) is about 3–4 eV for a shallow d energy level, and it also agrees well with the experimental result. The formula used to calculate $J^2_{s(p),d}(0, 0)$ based on Schrieffer–Wolff transformation is not suitable for a shallow d energy level [46], and the corresponding $NJ^2_{s(p),d}(0, 0)$ diverges when E_d approaches the valence band edge. In our calculation, the divergence difficulty is overcome, and a finite value for $J^n_{s(p),d}$ is obtained.

4.3. The $T_{dn\sigma}$ dependence of J_{dd}

It has been shown that the maximum of J_{dd} reaches about 4 meV in figure 3(b). The maximum can be considerably increased if a larger mixing parameter $T_{dn\sigma}$ is used. Since $T_{dn\sigma}$ is a parameter dependent on the particular material, it is necessary to consider the $T_{dn\sigma}$ dependence of J_{dd}. The value of $T_{dn\sigma}$ is in the range of 0.20–0.35 eV for II–VI DMS [45], but corresponding values for III–V DMS are rather scarce in the literature. Without loss of generality, the mixing
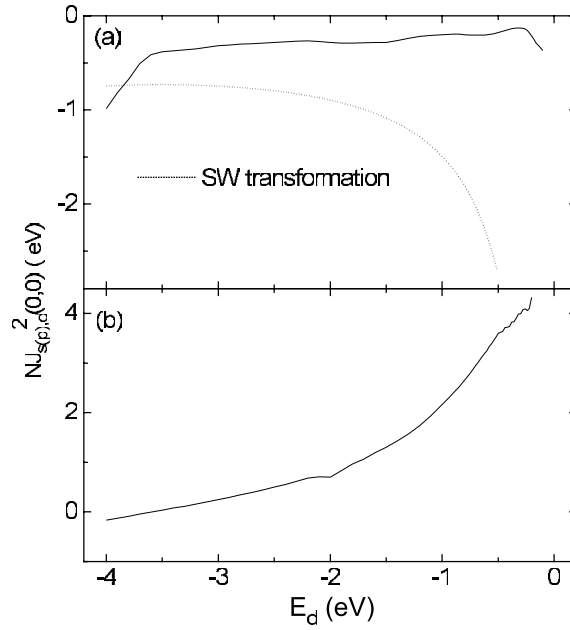
Figure 4. $NJ^2_{s(p),d}(0,0)$ as a function of E_d. $T_{dn\sigma}$ in equation (7) is 0.8 eV, and $T_{dn\sigma}$ in equations (8) is 0.2 eV. The corresponding result from Schrieffer–Wolff (SW) transformation is also shown for comparison [46]. The parameters for the valence band used for panels (a) and (b) are the same as those used for figures 2(a) and (b), respectively. The other parameters are the same as those for figure 3.
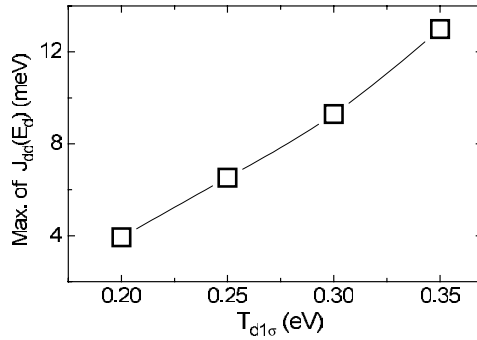

Figure 5. The maximum of $J_{dd}(E_d)$ as a function of $T_{d1\sigma}$ ($T_{d2\sigma} = \sqrt{2}T_{d1\sigma}$). The other parameters are the same as those for figure 3(b).

strength dependence of J_{dd} is investigated also in the range of 0.20–0.35 eV. Figure 5 shows the mixing strength dependence of the maximum of $J_{dd}(E_d)$, which increases with the mixing strength.

According to Larson's results, $T_{dn\sigma}(k)$ has a maximum at $k = 0$ and decreases in all directions away from $k = 0$, vanishing at the X point for II–VI DMS [45]. It may be a reasonable assumption that this conclusion is also appropriate for III–V DMS since they have the same zinc-blende crystal structure as II–VI DMS. Therefore, a larger $T_{dn\sigma}$ should be adopted in the calculation if E_d increases, since the corresponding resonant momentum decreases with E_d. This also means that $T_{dn\sigma}$ increases with E_d in real DMS.
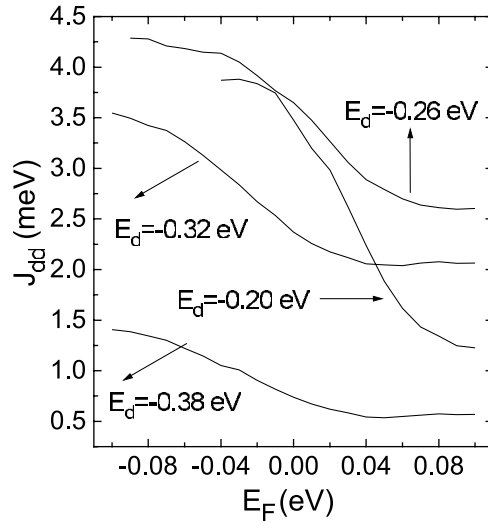
Figure 6. The exchange constant J_{dd} as a function of E_F. The parameters are the same as those for figure 3(b).

$T_{dn\sigma}$ depends sensitively on the microscopic environment. In the semiconductors with a zinc-blende structure, the valence band state can be regarded as a linear combination of sp^3 hybrid atomic orbital states. When magnetic impurity atoms occupy the Ga sites, there is an opportunity to obtain a large s(p)–d mixing strength $T_{dn\sigma}$ since the sp^3 orbital state has a strong orientation dependence. When magnetic impurity atoms occupy the interstitial sites, $T_{dn\sigma}$ should be small, because the volume overlap of the d state and sp^3 orbital state is small due to the orientation dependence of the sp^3 orbital state. The change of the lattice constant of the crystal also leads to a variation of $T_{dn\sigma}$. $T_{dn\sigma}$ usually increases with decreasing lattice constant, since the volume overlap of the d state and the sp^3 state also increases.

It has been shown that the location of Mn sites in Ga$_{1-x}$Mn$_x$As is affected by the annealing procedure [40]. Accompanying the change of Mn sites in the annealing procedure, the carrier density also shows a complicated change. The carrier density increased from 6×10^{20} to 1×10^{21} cm^{-3} for a Ga$_{1-x}$Mn$_x$As film annealed at 282 °C, the Curie temperature T_C also increases from 67 to 111 K, and the Mn interstitial concentration is reduced. On the other hand, a sample annealed at 350 °C showed no change in the hole concentration, but T_C decreased to 49 K, and the interstitial Mn and a significant fraction of the substitutional Mn form random precipitates [40]. This experiment shows that the concentration of substitutional Mn plays an important role in achieving strong ferromagnetism in III–V DMS. As discussed in the above paragraph, $T_{dn\sigma}$ decreases when Mn atoms move from their substitutional sites to interstitial sites or form certain random precipitates; hence T_C is decreased. The annealing effect cannot be explained by just the variation of the hole concentration, since T_C decreased to 49 K but the hole concentration was not changed when the sample was annealed at 350 °C. So the $T_{dn\sigma}$ dependence of J_{dd} may be helpful for interpreting these complicated phenomena.

4.4. The E_F dependence of J_{dd}

Figure 6 shows the E_F dependence of J_{dd}. J_{dd} increases when the Fermi energy E_F is decreased around the valence band top. However, the E_F dependence of J_{dd} becomes less significant if E_d is decreased. This result can be explained as reflecting the fact that the change of E_F cannot
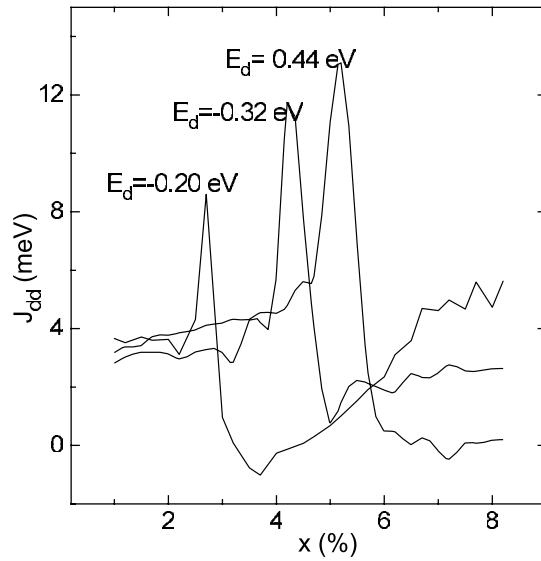
Figure 7. The impurity concentration (x) dependence of J_{dd}. The parameters are the same as those for figure 3(b).

lead to a significant variation of the centre of gravity of the state density for a relatively deep d energy level.

In a p-type semiconductor, E_F is in a gap and near E_v, and the p-type carrier density increases with decreasing E_F, so this result indicates that J_{dd} increases with the p-type carrier density [4, 26]. For $Ga_{1-x}Mn_xAs$ the carriers are provided by Mn atoms, and the carrier density is controlled by the Mn impurity concentration x, so J_{dd} increases with small x. In experiments, E_F can also be increased by doping Si into p-type $Ga_{1-x}Mn_xAs$, so J_{dd} decreases with the concentration of Si [41].

The ferromagnetism of DMS used to be explained as carrier-induced ferromagnetism, and this interpretation indicates that free carriers play an important role in the ferromagnetism in DMS. Some experimental results and theoretical works have proved this point. Dietl *et al* have calculated T_C for various DMS, and found that T_C increases with the free carrier density [26]. This point has been verified by some experimental results [22, 38]; however, some experimental results [20, 39] reveal that the dependence of T_C on the carrier density is not as significant as stated. The controversy may indicate that free carriers are not an essential factor for the ferromagnetism of DMS. In fact, ferromagnetism exists in p-type DMS and also in n-type DMS, and even in insulating 'DMS'.

In our quasiparticle method, the carrier concentration is not directly included as a parameter, but the Fermi energy E_F plays the same role as the carrier concentration in other models. It has been shown that only when E_F approaches the valence band edge and E_d is shallow enough can the change of E_F lead to a significant variation of the exchange constant J_{dd}. Hence only E_F is adjusted to an appropriate position [38]; the magnetism can be changed via change of the carrier concentration.

4.5. The impurity concentration dependence of J_{dd}

In DMS, the mean distance between 3d atoms decreases with x, so it is necessary to study the effect stemming from the variation of distance in our calculation. Figure 7 shows that J_{dd}

increases with small x, then reaches a maximum, and finally decreases sharply with x. The maximum position increases with decreased E_d. This phenomenon can be explained by the phase factor. Because the resonant momentum increases with decreasing E_d, the phase factor can be maintained at a fixed value by decrease of the mean distance or, alternatively, increase of x. For a relatively deep level and low concentration, such as $E_d = -0.44$ eV and $x < 5\%$, our results agree well with experimental results [23] and existing theoretical results [26, 27, 30]. However, for a relatively shallow level, such as $E_d = -0.20$ eV, an oscillatory dependence of J_{dd} on x emerges. The oscillatory phenomenon can be caused by several factors as explained in what follows.

  (i) The phase factor effect: since the mean distance between two magnetic impurities decreases with x, the phase factor depends on x.
 (ii) The filling factor effect: since the d energy is shallow, the filling factor is affected by x, and this will lead to an extra change of the centre of gravity of the d state.
(iii) Band-edge singularity: the point $\vec{k} = 0$ is a singularity for the density of the valence band states; a slight change of x may cause a significant variation of J_{dd} for a shallow d energy level.

The oscillatory dependence of J_{dd} on x indicates that J_{dd} may decrease with large x in some DMS, which have valence band structures similar to our double-valence-band model.

In experiments, the magnetic impurity concentration x not only means the average distance between magnetic atoms, but also determines other parameters, such as E_F (carrier density), so compensation and precipitation are usually considered in explaining the concentration dependence of T_C. It has been shown that the concentration dependence of T_C can be approximately described in terms of the corresponding hole concentration dependence of $Ga_{1-x}Mn_xAs$ [23]. There are some extreme cases, in which the hole density is low and is nearly independent of x, and the magnetic impurity concentration dependence of J_{dd} reveals a 'pure' distance dependence of J_{dd}. It has been shown that T_C increases linearly with x up to about 0.07 and decreases with x beyond 0.07 for $In_{1-x}Mn_xAs$ [39]. The reduced T_C observed beyond $x = 0.07$ is not due to a decrease in hole concentration since the hole concentration is nearly the same. This can be explained if one assumes that more Mn atoms exist in the forms of interstitials and random precipitates for x beyond 0.07 [40]. Another possibility is considering the distance dependence of J_{dd}. In fact, Slupinski *et al* have explained the ferromagnetism with relatively low hole concentration as a result of ferromagnetic local pairing. This indicates that the distance between magnetic atoms should be an independent factor, to be considered for III–V DMS.

4.6. Unsymmetrical broadening of the d state density

Figure 8 shows the local density for the point at $E_d = -0.20$ eV in figure 3(b) (the state densities for other points in figure 3(b) are similar and are not shown). Comparing figure 8 with figure 1, we find that the shape of the state density is very similar to the case for $\theta = 3\pi/4$ ($7\pi/4$) (θ is the phase factor of f_{di,d_1i_1}) in figure 1. Comparing the density in ferromagnetic alignment with that in antiferromagnetic alignment, we find that the broadening of the d state density is unsymmetrical. There are two contrary trends in the variation of the density: one is the broadening and decreasing of the density on the right of the quasiparticle peak; the other is the compaction of the density towards the high energy side on the left of the quasiparticle peak. The former trend primarily originates from the decrease of the d level lifetime, and facilitates ferromagnetism. The latter trend facilitates antiferromagnetism (superexchange).
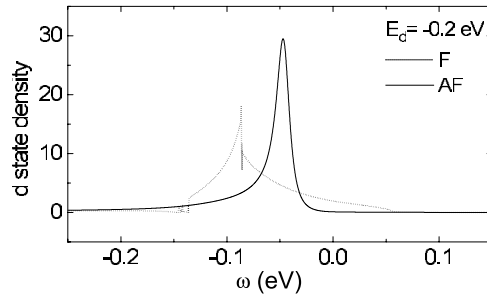
Figure 8. The density of local d states. The parameters are the same as those for figure 3(b).

In the example, the former trend gains advantage over the latter trend; hence ferromagnetism emerges.

The peak position of the $J_{dd}(E_d)$ curve in figure 3 can be explained by the unsymmetrical broadening of the d state density. If E_d is in the vicinity of the band top, the d state density in the F configuration can only be broadened towards the low energy side since the band state density tends to zero towards the high energy side, so ferromagnetism emerges. If E_d is in the vicinity of the band bottom, the d state density in the F configuration can only be broadened towards the high energy side since the band state density tends to zero towards the low energy side, so antiferromagnetism emerges.

In a sense, our model calculation can bridge the discrepancy between the double-exchange model and the Zener model. For $E_F < E_v$ and $E_d \to E_v$, the d level is partly filled, and d holes are produced. Since the d energy level is very shallow, the valence band electron is pushed away in the vicinity of the Fermi energy E_F (see equation (7)); a half-metallic state can be obtained, and therefore the double-exchange model may be appropriate for the case of a shallow energy level. For $E_F > E_v$ and a slightly deeper E_d, there are almost no d holes, and the ferromagnetism originates from the decrease of density on the high energy side; hence the Zener model may be more appropriate for the case of a relatively 'deep' energy level.

5. Conclusion

In summary, a quasiparticle method based on the s(p)–d mixing model is used for the study of ferromagnetism in III–V DMS. In comparison with other approaches, the quasiparticle method provides a general framework for incorporating other interactions [43], and it is suitable for a more extensive parameter region, e.g., from II–IV DMS to III–V DMS. The local d state density shows a lowering centre of gravity of the d level due to unsymmetrical broadening when ferromagnetism emerges in DMS. Our calculation demonstrates that a shallow d energy level, low Fermi energy level, large s(p)–d mixing strength and appropriate magnetic impurity concentration are important for achieving a strong ferromagnetism in III–V DMS. Relevant experimental results, especially ones that are difficult to understand in the framework of existing models, are interpreted on the basis of our calculation.

Acknowledgments

Appendix A. A detailed derivation of the Green function $\langle\langle\hat{a}_{di\sigma}|\hat{a}_{d'i'\sigma'}^{\dagger}\rangle\rangle$

In the Hartree–Fock approximation, $\sum_{di\sigma} U_d\langle\hat{n}_{di\bar{\sigma}}\rangle\hat{n}_{di\sigma}$ ($\langle\cdots\rangle$ denotes the thermal average) is substituted for the Hubbard repulsion term $\frac{1}{2}\sum_{di\sigma} U_d\hat{n}_{di\sigma}\hat{n}_{di\bar{\sigma}}$ in equation (1), so the s(p)–d mixing Hamiltonian is rewritten as

$$\hat{H} = \sum_{di\sigma} E_d\hat{n}_{di\sigma} + \sum_{di\sigma} U_d\langle\hat{n}_{di\bar{\sigma}}\rangle\hat{n}_{di\sigma} + \sum_{nk\sigma} E_{nk}^e\hat{c}_{nk\sigma}^{\dagger}\hat{c}_{nk\sigma}$$

$$+ \frac{1}{\sqrt{N}}\sum_{dink\sigma}(T_{dn\sigma}\mathrm{e}^{\mathrm{i}\vec{k}\cdot\vec{r}_i}\hat{a}_{di\sigma}^{\dagger}\hat{c}_{nk\sigma} + T_{dn\sigma}^*\mathrm{e}^{-\mathrm{i}\vec{k}\cdot\vec{r}_i}\hat{c}_{nk\sigma}^{\dagger}\hat{a}_{di\sigma}). \tag{A.1}$$

The equation of motion for a retarded Green function $\langle\langle\hat{A}|\hat{B}\rangle\rangle$ takes the form [57–59]

$$\omega\langle\langle\hat{A}|\hat{B}\rangle\rangle = \langle\{\hat{A},\hat{B}\}\rangle + \langle\langle[\hat{A},\hat{H}]|\hat{B}\rangle\rangle, \tag{A.2}$$

where $\hat{A}$, $\hat{B}$ are any two operators, and $\{\hat{A},\hat{B}\}$ denotes $\hat{A}\hat{B}+\hat{B}\hat{A}$ and $[\hat{A},\hat{B}]$ denotes $\hat{A}\hat{B}-\hat{B}\hat{A}$. In this paper we adopt the notation $\langle\langle\hat{A}|\hat{B}\rangle\rangle$ instead of $\langle\langle\hat{A};\hat{B}\rangle\rangle$ for the Fourier frequency transform of the double-time retarded Green function $\langle\langle\hat{A}(t);\hat{B}(t')\rangle\rangle$ [59].

According to equation (A.2), we can write down the following two equations:

$$(\omega - E_d - U_d\langle\hat{n}_{di\bar{\sigma}}\rangle)\langle\langle\hat{a}_{di\sigma}|a_{d'i'\sigma'}^{\dagger}\rangle\rangle = \delta_{di\sigma,d'i'\sigma'} + \frac{1}{\sqrt{N}}\sum_{nk}T_{dn\sigma}\mathrm{e}^{\mathrm{i}\vec{k}\cdot\vec{r}_i}\langle\langle\hat{c}_{nk\sigma}|a_{d'i'\sigma'}^{\dagger}\rangle\rangle, \tag{A.3}$$

$$(\omega - E_{nk}^e)\langle\langle\hat{c}_{nk\sigma}|a_{d'i'\sigma'}^{\dagger}\rangle\rangle = \frac{1}{\sqrt{N}}\sum_{d_1 i_1}T_{d_1 n\sigma}^*\mathrm{e}^{-\mathrm{i}\vec{k}\cdot\vec{r}_{i_1}}\langle\langle\hat{a}_{d_1 i_1\sigma}|a_{d'i'\sigma'}^{\dagger}\rangle\rangle. \tag{A.4}$$

Eliminating $\langle\langle\hat{c}_{nk\sigma}|\hat{a}_{d'i'\sigma'}^{\dagger}\rangle\rangle$ from equations (A.3) and (A.4), we obtain equation (2).

Introducing an effective field $\Sigma(di\sigma)$, we can write equation (2) in another form:

$$(\omega - \Sigma(di\sigma))\langle\langle\hat{a}_{di\sigma}|\hat{a}_{d'i'\sigma'}^{\dagger}\rangle\rangle = \delta_{di\sigma,d'i'\sigma'} + (e_{di\sigma} - \Sigma(di\sigma))\langle\langle\hat{a}_{di\sigma}|\hat{a}_{d'i'\sigma'}^{\dagger}\rangle\rangle$$

$$+ \sum_{d_1 i_1\neq di} f_{di,d_1 i_1}(\sigma)\langle\langle\hat{a}_{di\sigma}|\hat{a}_{d'i'\sigma'}^{\dagger}\rangle\rangle. \tag{A.5}$$

Taking $\langle\langle\hat{a}_{di\sigma}|\hat{a}_{d'i'\sigma'}^{\dagger}\rangle\rangle$ determined from equation (A.5) back into equation (A.5), we obtain

$$(\omega - \Sigma(di\sigma))\langle\langle\hat{a}_{di\sigma}|\hat{a}_{d'i'\sigma'}^{\dagger}\rangle\rangle = \delta_{di\sigma,d'i'\sigma'}$$

$$+ \left(e_{di\sigma} - \Sigma(di\sigma) + \sum_{d_1 i_1\neq di}\frac{f_{di,d_1 i_1}(\sigma)f_{d_1 i_1,di}(\sigma)}{\omega - \Sigma(d_1 i_1\sigma)}\right)\langle\langle\hat{a}_{di\sigma}|\hat{a}_{d'i'\sigma'}^{\dagger}\rangle\rangle$$

$$+ \sum_{d_1 i_1\neq di}\frac{f_{di,d_1 i_1}(\sigma)(e_{d_1 i_1\sigma} - \Sigma(d_1 i_1\sigma))}{\omega - \Sigma(d_1 i_1\sigma)}\langle\langle\hat{a}_{d_1 i_1\sigma}|\hat{a}_{d'i'\sigma'}^{\dagger}\rangle\rangle$$

$$+ \sum_{\substack{d_1 i_1\neq di\\ d_2 i_2\neq d_1 i_1,di}}\frac{f_{di,d_1 i_1}(\sigma)f_{d_1 i_1,d_2 i_2}(\sigma)}{\omega - \Sigma(d_1 i_1\sigma)}\langle\langle\hat{a}_{d_2 i_2\sigma}|\hat{a}_{d'i'\sigma'}^{\dagger}\rangle\rangle. \tag{A.6}$$

If we require

$$\Sigma(di\sigma) = e_{di\sigma} + \sum_{d_1 i_1\neq di}\frac{f_{di,d_1 i_1}(\sigma)f_{d_1 i_1,di}(\sigma)}{\omega - \Sigma(d_1 i_1\sigma)}, \tag{A.7}$$

and omit the last two terms, then

$$(\omega - \Sigma(di\sigma))\langle\langle\hat{a}_{di\sigma}|\hat{a}_{d'i'\sigma'}^{\dagger}\rangle\rangle \approx \delta_{di\sigma,d'i'\sigma'}. \tag{A.8}$$

The method for expanding the Green function shares the idea of the CPA for binary alloy theory [47]. In binary alloy theory, an effective propagator $\overline{G}$ is also used to expand the Green function G, and G takes the form

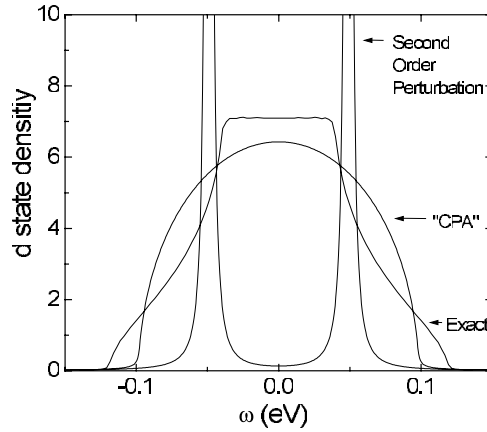$$G = \overline{G} + \overline{G}\,\overline{T}\,\overline{G}, \tag{A.9}$$

Figure A.1. A comparison between various solutions for the TBH. $t = 0.02$ eV, which is close to $f_{di,d_1 i_1}(\sigma)$, is assumed. The CPA solution can characterize well the essence of the extended state in the TBH.

where $\overline{T}$ is usually called the T-matrix, which is written as

$$\overline{T} = \overline{V} + \overline{V}\,\overline{G}\,\overline{T}, \tag{A.10}$$

where $\overline{V}$ is the difference between the real Hamiltonian $\hat{H}$ and the effective Hamiltonian. If $\overline{T} = 0$, then $G = \overline{G}$. However, it is usually difficult to resolve $\overline{T} = 0$ exactly, and some approximations are used. For the binary alloy problem, $\overline{V}$ is decomposed into $\overline{v}_1$ and $\overline{v}_2$; $\overline{T}$ is also decomposed into $\overline{t}_1$ and $\overline{t}_2$, and $\overline{T} = 0$ is approximated as

$$\sum_{i=1,2} c_i \overline{t}_i = 0, \tag{A.11}$$

where c_i is the concentration of the ith constituent. In our problem the situation is more complicated: $f_{di,d_1 i_1}(\sigma)$ has more possible values, and the approximation of the binary alloy problem is not applicable here. Here an approximation

$$\overline{T}_{di\sigma,di\sigma} = e_{di\sigma} - \Sigma(di\sigma) + \sum_{d_1 i_1 \neq di} \frac{f_{di,d_1 i_1}(\sigma) f_{d_1 i_1, di}(\sigma)}{\omega - \Sigma(d_1 i_1 \sigma)} \tag{A.12}$$

is adopted for evaluating $\overline{T}$. Further considering averaging over a random distribution of magnetic atoms and requiring $T_{di\sigma,di\sigma} = 0$, we obtain equation (6). In this paper we also use CPA as the name for the approximation.

The validity of this approximation is tested here. A tight binding Hamiltonian (TBH) $\hat{H} = \sum_{\langle i,j \rangle} t a_i^\dagger a_j$ and an ordered, simple cubic lattice are used to calculate the local state density. The exact solution can be obtained through a transformation of $\hat{a}_i = (1/\sqrt{N}) \sum_k \mathrm{e}^{-i\vec{k}\cdot\vec{r}_i} \hat{a}_k$. Another possible approach is via perturbative expansion, where the 'bare' propagator ω^{-1} is used. The second-order perturbative solution can be obtained from equation (A.7) where zero takes the place of $e_{di\sigma}$, t takes the place of $f_{di,d_1 i_1}$, and ω takes the place of $\omega - \Sigma(d_1 i_1 \sigma)$. Figure A.1 shows the local state densities from the exact solution, the CPA solution, and the second-order perturbative solution. In comparison with the exact solution, our CPA one is more believable than that from the second-order perturbative approximation. This may be an important reason that only very weak ferromagnetism [60] was obtained in the conventional perturbative approach [45].

Appendix B. Details on the averaging in the CPA

In this appendix the details on the averaging over a random distribution of magnetic atoms are presented.

First we should consider the averaging in the subspace of spin freedom. For an operator $\hat{X}(\sigma)$, it can be expressed as two pure numbers $X(1)$, $X(2)$ in its local spin representation. Suppose that the angle between the local spin axis and the global spin axis is θ; then $\langle\uparrow |X|\uparrow\rangle$, $\langle\downarrow |X|\downarrow\rangle$ in the global spin representation can be written as

$$\begin{aligned}
\langle\uparrow |X|\uparrow\rangle &= \cos^2(\theta/2)X(1) + \sin^2(\theta/2)X(2),\\
\langle\downarrow |X|\downarrow\rangle &= \sin^2(\theta/2)X(1) + \cos^2(\theta/2)X(2).
\end{aligned} \tag{B.1}$$

Further, we need to find a distribution function to describe the random distribution of magnetic atoms. Suppose that the probability of a site being occupied by a magnetic atom is p_l on a crystal axis; then the probability of a site not being occupied is $1 - p_l$, so the distance i between two nearest magnetic atoms exhibits the following distribution:

$$P(i) = p_l(1 - p_l)^{i-1} \qquad (i = 1, 2, \ldots). \tag{B.2}$$

We are ready to show that the distribution has the properties

$$\begin{aligned}
\sum_{i=1}^{\infty} P(i) &= 1,\\
\sum_{i=1}^{\infty} P(i)i &= 1/p_l.
\end{aligned} \tag{B.3}$$

If the concentration of magnetic atoms is x, the mean separation of magnetic atoms is $x^{-1/3}$. Let $p_l = x^{1/3}$; then $P(i)$ can describe well the random distribution of magnetic atoms.

There exist many crystal axes with different minimal separations; a variety of crystal axes should be included in the summation in equation (6). In our actual calculation, only $\langle 100\rangle$, $\langle 010\rangle$, $\langle 001\rangle$ are considered, and the others are neglected since a series of simplifications have been made in our model calculation.

Appendix C. The approximate expression for f_{di,d_1i_1}

The dispersion of a simple cubic energy band takes the form

$$E_{nk} = E_n + 2T_n(\cos(k_x) + \cos(k_y) + \cos(k_z)), \tag{C.1}$$

where the unit of k is $1/a$ and a is the lattice constant. Constructing a power series expansion and omitting terms higher than the second-order ones, we can write E_{nk} as

$$E_{nk} = E_n + 6T_n - T_n k^2 \tag{C.2}$$

in the vicinity of the band top. There is a similar expansion for the k points in the vicinity of the band bottom.

Taking the approximate expression for E_{nk} into equation (8), we can write

$$f_{di,d_1i_1}(\sigma) = \sum_n \frac{T_{dn\sigma} T^*_{d_1n\sigma}}{T_n} F(a_n, b_n, r), \tag{C.3}$$

where $a_n + ib_n = \left[\omega - E_n - 6T_n - \frac{1}{N}\sum_{di} \frac{|T_{dn\sigma}|^2}{\omega - \Sigma(di\sigma)}\right]/(-T_n)$ and $F(a_n, b_n, r)$ is an integral that takes the form

$$F(a_n, b_n, r) = \frac{1}{(2\pi)^3} \int_{\vec{k}\in 1BZ} \frac{e^{i\vec{k}\cdot\vec{r}}\, d^3k}{k^2 - (a_n + ib_n)}. \tag{C.4}$$

It is convenient to evaluate the integral defined by equation (C.4) in spherical coordinates. Taking the θ and φ integrations first,

$$F(a_n, b_n, r) = \frac{1}{4\pi^2 \mathrm{i} r} \int_{-\pi}^{\pi} \frac{k \mathrm{e}^{\mathrm{i}kr} \, \mathrm{d}k}{k^2 - (a_n + \mathrm{i}b_n)}. \tag{C.5}$$

Because the main contribution comes from the k points in the vicinity of the pole, the limits of the integral can be extended to infinity; hence,

$$F(a_n, b_n, r) \approx \frac{1}{4\pi^2 \mathrm{i} r} \int_{-\infty}^{\infty} \frac{k \mathrm{e}^{\mathrm{i}kr} \, \mathrm{d}k}{k^2 - (a_n + \mathrm{i}b_n)} = \frac{1}{4\pi r} \mathrm{e}^{\mathrm{i}k_n r}, \tag{C.6}$$

where k_n is the root of the equation $k^2 = a_n + \mathrm{i}b_n$ in the upper complex half-plane.

References

[1] Munekata H, Ohno H, von Molnar S, Segmüller A, Chang L L and Esaki L 1989 *Phys. Rev. Lett.* **63** 1849
[2] Ohno H, Shen A, Matsukura F, Oiwa A, Endo A, Katsumoto S and Iye Y 1996 *Appl. Phys. Lett.* **69** 363
[3] Hayashi T, Tanaka M, Nishinaga T, Shimada H, Tsuchiya H and Otuka Y 1997 *J. Cryst. Growth* **175/176** 1063
[4] Van Esch A, Van Bockstal L, Boeck J De, Verbanck G, van Steenbergen A S, Wellmann P J, Grietens B, Bogaerts R, Herlach F and Borghs G 1997 *Phys. Rev.* B **56** 13103
[5] Koshihara S, Oiwa A, Hirasawa M, Katsumoto S, Iye Y, Urano C, Takagi H and Munekata H 1997 *Phys. Rev. Lett.* **78** 4617
[6] Ohno H, Akiba N, Matsukura F, Shen A, Ohtani K and Ohno Y 1998 *Appl. Phys. Lett.* **73** 363
[7] Ohno H 1998 *Science* **281** 951
[8] Reed M L, El-Masry N A, Stadelmaier H H, Ritums M K, Reed M J, Parker C A, Roberts J C and Bedair S M 2001 *Appl. Phys. Lett.* **79** 3473
[9] Sonoda S, Shimizu S, Sasaki T, Yamamoto Y and Hori H 2002 *J. Cryst. Growth* **237–239** 1358
[10] Thaler G T, Overberg M E, Gila B, Frazier R, Abernathy C R, Pearton S J, Lee J S, Lee S Y, Park Y D, Khim Z G, Kim J and Ren F 2002 *Appl. Phys. Lett.* **80** 3964
[11] Park S E, Lee H-J, Cho Y C, Jeong S-Y, Cho C R and Cho S 2002 *Appl. Phys. Lett.* **80** 4187
[12] Blattner A J and Wessels B W 2002 *J. Vac. Sci. Technol.* B **20** 1582
[13] Park W K, Ortega-Hertogs R J, Moodera J S, Punnoose A and Seehra M S 2002 *J. Appl. Phys.* **91** 8093
[14] Zajac M, Gosk J, Kaminska M, Twardowski A, Szyszko T and Podsiadlo S 2001 *Appl. Phys. Lett.* **79** 2432
[15] Kuwabara S, Ishii K, Haneda S, Kondo T and Munekata H 2001 *Physica* E **10** 233
[16] Szyszko T, Kamler G, Strojek B, Weisbrod G, Podsiadło S, Adamowicz L, Gębicki W, Szczytko J, Twardowski A and Sikorski K 2001 *J. Cryst. Growth* **233** 631
[17] Tiwari A, Jin C, Kvit A, Kumar D, Muth J F and Narayan J 2002 *Solid State Commun.* **121** 371
[18] Liu Z, Boeck J De, Moshchalkov V V and Borghs G 2002 *J. Magn. Magn. Mater.* **242–245** 967
[19] Dyck J S, Hájek P, Lošt'ák P and Uher C 2002 *Phys. Rev.* B **65** 115212
[20] Pearton S J, Overberg M E, Thaler G, Abernathy C R, Theodoropoulou N, Hebard A F, Chu S N G, Wilson R G, Zavada J M, Polyakov A Y, Osinsky A V, Norris P E, Chow P P, Wowchack A M, Van Hove J M and Park Y D 2002 *J. Vac. Sci. Technol.* A **20** 721
[21] Saito H, Zaets W, Yamagata S, Suzuki Y and Ando K 2002 *J. Appl. Phys.* **91** 8085
[22] Fukuma Y, Asada H, Arifuku M and Koyanagi T 2002 *Appl. Phys. Lett.* **80** 1013
[23] Matsukura F, Ohno H, Shen A and Sugawara Y 1998 *Phys. Rev.* B **57** R2037
[24] For recent theoretical review, see König J, Schliemann J, Jungwirth T and MacDonald A H 2003 *Electronic Structure and Magnetism of Complex Materials* ed D J Singh and D A Papaconstantopoulos (Berlin: Springer) p 163
[25] Akai H 1998 *Phys. Rev. Lett.* **81** 3002
[26] Dietl T, Ohno H, Matsukura F, Cibert J and Ferrand D 2000 *Science* **287** 1019
[27] Dietl T, Matsukura F and Ohno H 2002 *Phys. Rev.* B **66** 033203
[28] König J, Lin H-H and MacDonald A H 2000 *Phys. Rev. Lett.* **84** 5628
[29] Inoue J, Nonoyama S and Itoh H 2000 *Phys. Rev. Lett.* **85** 4610
[30] Litvinov V I and Dugaev V K 2001 *Phys. Rev. Lett.* **86** 5593
[31] Sanvito S, Ordejón P and Hill N A 2001 *Phys. Rev.* B **63** 165206
[32] Kulatov E, Nakayama H, Mariette H, Ohta H and Uspenskii Yu A 2002 *Phys. Rev.* B **66** 045203
[33] Kronik L, Jain M and Chelikowsky J R 2002 *Phys. Rev.* B **66** 041203(R)

[34] Zener C 1951 *Phys. Rev.* **82** 403
[35] Anderson P W and Hasegawa H 1955 *Phys. Rev.* **100** 675
[36] Zener C 1951 *Phys. Rev.* **81** 440
[37] Theodoropoulou N, Hebard A F, Overberg M E, Abernathy C R, Pearton S J, Chu S N G and Wilson R G 2001
        Appl. Phys. Lett. **79** 3473
[38] Matsukura F, Chiba D, Omiya T, Abe E, Dietl T, Ohno Y, Ohtani K and Ohno H 2002 *Physica* E **12** 351
[39] Slupinski T, Oiwa A, Yanagi S and Munekata H 2002 *J. Cryst. Growth* **237–239** 1326
[40] Yu K M, Walukiewicz W, Wojtowicz T, Kuryliszyn I, Liu X, Sasaki Y and Furdyna J K 2002 *Phys. Rev.* B **65**
        201303(R)
[41] Beschoten B, Crowell P A, Malajovich I, Awschalom D D, Matsukura F, Shen A and Ohno H 1999 *Phys. Rev.*
        Lett. **83** 3073
[42] Anderson P W 1961 *Phys. Rev.* **124** 41
[43] Cai J H and Liu G Q 2002 *Phys. Rev.* B **66** 064411
[44] Leder H J and Mühlschlegel B 1978 *Z. Phys.* B **29** 341
[45] Larson B E, Hass K C, Ehrenreich H and Carlsson A E 1988 *Phys. Rev.* B **37** 4137
[46] Schrieffer J R and Wolff P A 1966 *Phys. Rev.* **149** 491
[47] Soven P 1967 *Phys. Rev.* **156** 809
[48] Liechtenstein A I, Katsnelson M I, Antropov V P and Gubanov V A 1987 *J. Magn. Magn. Mater.* **67** 65
[49] Oguchi T, Terakura K and Hamada N 1983 *J. Phys. F: Met. Phys.* **13** 145
      Oguchi T, Terakura K and Williams A R 1983 *Phys. Rev.* B **28** 6443
[50] Chelikowsky J R and Cohen M L 1976 *Phys. Rev.* B **14** 556
[51] Qu H, Nilsson P O, Kanski J and Ilver L 1989 *Phys. Rev.* B **39** 5276
[52] Agrawal B K and Agrawal S 1992 *Phys. Rev.* B **45** 8321
[53] Okabayashi J, Kimura A, Rader O, Mizokawa T, Fujimori A, Hayashi T and Tanaka M 2001 *Physica* E **10** 192
[54] Okabayashi J, Kimura A, Rader O, Mizokawa T, Fujimori A, Hayashi T and Tanaka M 2001 *Phys. Rev.* B **64**
        125304
[55] Asklund H, Ilver L, Kanski J, Sadowski J and Mathieu R 2002 *Phys. Rev.* B **66** 115319
[56] Twardowski A 1999 *Mater. Sci. Eng.* B **63** 96
[57] Zubarev D N 1960 *Sov. Phys.—Usp.* **3** 320 (Engl. Transl.)
[58] Roth Laura M 1969 *Phys. Rev.* **184** 451
[59] Li Z 1985 *Solid State Theory* (Beijing: Higher Education Press) p 371 (Chinese version)
[60] Blinowski J, Kacman P and Majewski J A 1996 *Phys. Rev.* B **53** 9524